Clinical Biochemistry 72 (2019) 58–63

Contents lists available at ScienceDirect

Clinical Biochemistry

journal homepage: www.elsevier.com/locate/clinbiochem

Blood-based molecular signature of Alzheimer's disease *via* spectroscopy and metabolomics☆

Lucie Habartová[a,*], Kateřina Hrubešová[a], Kamila Syslová[b], Jana Vondroušová[b], Zdeněk Fišar[c], Roman Jirák[c], Jiří Raboch[c], Vladimír Setnička[a]

[a] Department of Analytical Chemistry, University of Chemistry and Technology Prague, Technická 5, 166 28 Prague 6, Czech Republic
[b] Department of Organic Technology, University of Chemistry and Technology Prague, Technická 5, 166 28 Prague 6, Czech Republic
[c] Department of Psychiatry, First Faculty of Medicine of the Charles University and General University Hospital in Prague, Ke Karlovu 11, 120 00 Prague 2, Czech Republic

A B S T R A C T

Objectives: With over 35 million cases worldwide, Alzheimer's disease (AD) represents the main cause of dementia. The differentiation of AD from other types of dementia is challenging and its early diagnosis is complicated. The established biomarkers are not only based on the invasive collection of cerebrospinal fluid, but also lack sufficient sensitivity and specificity. Therefore, much current effort is aimed at the identification of new biomarkers of AD in peripheral blood.

Design and methods: We focused on blood-based analyses using chiroptical spectroscopy (Raman optical activity, electronic circular dichroism) supplemented with conventional vibrational spectroscopy (infrared, Raman) and metabolomics (high-performance liquid chromatography with a high-resolution mass detection).

Results: This unique approach enabled us to identify the spectral pattern of AD and variations in metabolite levels. Subsequent linear discriminant analysis of the spectral data resulted in differentiation between the AD patients and control subjects.

Conclusions: It may be stated that this less invasive approach has strong potential for the identification of disease-related changes within essential plasmatic biomolecules and metabolites.

1. Introduction

As the global population ages, the number of patients suffering from different types of neurodegeneration continues to increase. In 2010, the total number of people with dementia was estimated at 35.6 million worldwide, a figure that is projected to reach 115 million by 2050 [1]. Alzheimer's disease (AD) represents the most common form of dementia, accounting for 60–70% of all cases and; thus, it is becoming one of the most problematic and costly diseases for the society [2].

Although genetic [3] and environmental influences [4] on AD have been evaluated and several biological hypotheses formulated to explain the cause of the disease (acetylcholine deficiency [5,6], amyloid beta (Aβ) overproduction [7,8], tau hyperphosphorylation [9,10], mitochondrial dysfunction [11] and others [12]), the etiology of the disease is still not well understood. AD is usually diagnosed from patient history, collateral family history and clinical observations based on the presence of characteristic neurological and neuropsychological features [13]. Despite this comprehensive and demanding approach, the diagnosis of AD carries a large percentage of uncertainty.

To obtain results of higher reliability, it is necessary to combine neuropsychological evaluation with biomarker measurement and brain visualization *via* various imaging methods, such as magnetic resonance imaging (MRI) or positron emission tomography (PET) [14–16]. Nevertheless, brain imaging is limited because these methods are either expensive, invasive, time-consuming and lack sensitivity to early stages of AD. The measurement of biomarker levels is also complicated. The established biomarker panel (Aβ and tau proteins) is assessed from cerebrospinal fluid (CSF) [17], the collection of which is burdensome for the patients. In addition, Aβ and tau proteins do not fulfil the requirements for an “appropriate” biomarker of AD, the sensitivity and specificity of which would ideally exceed 85% and 75%, respectively.

Many recent studies [18–20] have shown that other biomolecules, such as phospholipids, glutamate, creatine and serine, vary with AD progression. Moreover, a large number of these biomolecules are even found in significantly higher concentrations in peripheral blood than in CSF. Therefore, the analysis of blood plasma as a whole (containing all molecules, not only focusing on Aβ and tau proteins) and other biofluids seems to offer great potential for AD diagnostics at the molecular level. In fact, variations within plasmatic biomolecules are able to point to the multi-molecular signature of the disease [21]. Furthermore, as blood-based testing will most likely be a prerequisite for a future sensitive screening of large populations at risk of AD and a baseline in the

☆ Clinical Biochemistry – Special Issue dedicated to Workshop Alzheimer's Disease – Making the Point, 13. 11. 2018, Prague

* Corresponding author.
E-mail address: Lucie.Habartova@vscht.cz (L. Habartová).

https://doi.org/10.1016/j.clinbiochem.2019.04.004
Received 29 March 2019; Accepted 3 April 2019
Available online 04 April 2019

diagnostic approach thereto, it seems sensible to focus on the analysis of such clinical samples using the existing methods.

For example, methods of vibrational spectroscopy may serve as a standard screening tool in clinical laboratory analysis because they measure the chemical variations of structure and composition on the molecular level and are fast, minimally invasive and usually reagent-free. In addition, spectroscopic methods provide spectra that may contain information about the whole sample composition from proteins, peptides and lipids to electrolytes and hormones [21,22]. One of the methods newly introduced into the diagnosis of AD is infrared (IR) spectroscopy [23–25]. However, sensitivities and specificities vary significantly within particular studies, the data from which has typically not been cross-validated. In principle, even studies that claim high sensitivity and specificity cannot be practically applied to the reliable diagnosis of AD.

Chiroptical methods, specifically electronic circular dichroism (ECD) and Raman optical activity (ROA), are more suited to monitoring structural and stereochemical changes in blood plasma [26–29]. The principle of ECD and ROA is a different interaction of left- and right-handed circularly polarized radiation with chiral molecules, which makes these spectroscopic methods inherently sensitive to the 3D structure and spatial arrangement [30–32]. While ECD reflects the overall skeletal conformation of chiral compounds by means of a chromophore, ROA focuses on particular bond types and; thus, reveals the structural details. In addition to the peptide-backbone bands from regular secondary structure elements, such as α-helices and β-sheets, the ROA spectra contain distinct bands from loops and turns, thereby also providing information on the tertiary structure [31,33].

In our previous studies [34–36], we have shown that the unique simultaneous use of ECD, ROA and non-polarized methods of molecular spectroscopy contributes to a clearer understanding of the structural and stereochemical changes within blood plasma. The innovative methodology [26–28] enabled us to smoothly measure complex blood plasma samples and, consequently, reveal the specific molecular signature of type 1 diabetes mellitus [34], colon cancer [35] or pancreatic cancer [36]. In the latter case, metabolomics was also used to clearly identify molecules, the presence/absence of which may be a sign of developing pancreatic neoplasms. In this work, the aforementioned combination of spectroscopic and metabolomics techniques is employed to detect the structural alterations of plasmatic biomolecules and to identify metabolites that are associated with AD. Moreover, we believe that this approach will help to identify blood-based biomarkers with sensitivity and specificity high enough to facilitate the diagnosis of AD.

2. Experimental

2.1. Subjects

Patients suffering from AD ($n = 35$) were selected at the Department of Psychiatry of the General University Hospital in Prague and non-demented elderly controls (EC; $n = 29$) were recruited from the University of the Third Age within the Charles University in Prague after visiting the outpatient clinic. The average age of the AD patients and controls was 79 ± 8 and 67 ± 6 years, respectively. For including into the study, the AD patients were examined according to established diagnostic standards using a combination of psychological evaluation (Mini-mental state examination; MMSE [37]), CT and MRI scans and a routine biochemical blood test. Identical testing was performed for the EC group.

All study participants provided a signed informed consent. The study was conducted according to the principles expressed in the Declaration of Helsinki and approved by the Ethics Committee of the General University Hospital in Prague.

2.2. Blood plasma

Venous blood (9 mL) was collected from all study participants using sterile, anticoagulant-treated (K3EDTA) blood collection tubes (BD Vacutainer Systems, UK) at the Department of Psychiatry of the General University Hospital in Prague. Subsequently, the blood samples were centrifuged at 1500 × *g* for 10 min to obtain the plasma fractions, which were frozen immediately (−80 °C). Prior to each analysis at the University of Chemistry and Technology Prague, the plasma samples were thawed at room temperature and filtered through a membrane with a porosity of 0.45 μm (Grace, USA) at 13,000 × *g* for 10 min.

2.3. Electronic circular dichroism

The ECD experiments were conducted using the J-815 spectrometer (Jasco, Japan) operating in the UV-VIS spectral region. For measurements at lower wavelengths, a sterile phosphate buffer of plasma-identical pH = 7.4 was used to dilute the filtered samples in a volume ratio of 1:3. The diluted samples (25 μL) were placed into a quartz optical cell with a path length of 0.01 mm (Hellma, Germany), and measured within 185–280 nm. Sample temperature (23 °C) was controlled by a Peltier cell holder. Six scans with a data pitch of 0.1 nm were acquired for each sample and averaged in the Spectra Analysis module of the Spectra Manager program, ver. 2.6.0.1 (Jasco, Japan). No additional corrections were applied onto the spectra.

2.4. Raman optical activity and Raman spectroscopy

The Chiral*RAMAN-2X* spectrometer (BioTools, Inc., USA) equipped with an Opus 2 W/mpc6000 laser system (Laser Quantum, UK) with an excitation wavelength of 532 nm, and operating in a scattered circular polarization mode was used for the simultaneous acquisition of the Raman and ROA spectra. The filtered plasma samples (100 μL) were placed into a 4 × 4 mm optical cell (BioTools, Inc., USA) and measured at a Peltier-controlled temperature of 15 °C to avoid sample degradation. The acquisition of the ROA/Raman spectra with a resolution of ~7 cm^{-1} within 2500–90 cm^{-1} required a specific procedure. The procedure was developed in our laboratory [28] and it comprised of the addition of 10 mg NaI per 100 μL plasma for fluorescence quenching, sample photobleaching at 280 mW (real laser power on the sample) for 12 h and spectra acquisition at 250 mW for 24 h. The illumination period for the measurements was set to 1–2.5 s according to the optimal working range of the CCD detector and depending on individual samples. The laser power on the sample was monitored with a 1916-R optical power meter with an 818-P sensor (Newport Corporation, USA). To correct the residual baseline distortion in the raw ROA/Raman spectra, fast Fourier transform filter and a modified procedure from the literature were used [28,38].

2.5. Infrared spectroscopy

The FTIR spectra were collected on the Nicolet 6700 FTIR spectrometer (Thermo Scientific, USA). The filtered plasma samples (15 μL) were analysed on an ATR element (ZnSe) without any additional pretreatment. Each spectrum was created from 512 scans with a resolution of 4 cm^{-1} in the mid-IR region (4000–400 cm^{-1}). Water and water vapour spectra were acquired under identical conditions and subtracted from all sample spectra. Linear baseline correction was performed in the OMNIC 32 program, ver. 8.2 (Thermo Scientific, USA).

2.6. Metabolomics

Metabolomics was performed for randomly selected AD patients ($n = 20$) and controls ($n = 13$). The plasma samples were subjected to a multi-marker screening, that is, metabolites of diagnostic significance for AD were identified.

Acetonitrile (200 µL) was added to the room temperature-thawed plasma samples as an extraction solution. After homogenization and sonication at room temperature for 10 min, the solution was centrifuged at 6500 × *g* and 4 °C. The supernatant was analysed without further processing.

A liquid chromatography electrospray high-resolution mass spectrometry (LC-ESI-HRMS) system consisting of an Accela 600 pump, Accela autosampler and an LTQ Orbitrap Velos mass spectrometer (Thermo Scientific, USA) was used for the multi-marker screening. The separation was carried out at the Gemini C18-NX column (150 mm × 2 mm × 5 µm; Phenomenex, USA) with a mobile phase containing a 10-mM aqueous solution of ammonium acetate (solvent A) and acetonitrile (solvent B) in a gradient elution. The HPLC program was executed as 90% A for 5 min followed by 10% A (linear decrease over 15 min, held for 10 min) and 90% A (linear increase over 5 min, held for 10 min). The flow rate on the column was 200 µL min^{-1} and the sample injection volume was 10 µL. The mass spectrometer was operated in negative (ESI^-) and positive (ESI^+) electrospray ionization modes, as well as in a full scan mode (100–2000 Da) with high resolution (> 50,000). The MS experimental conditions were as follows: a spray voltage of 3000 V, ion transfer tube and HESI vaporizer temperatures of 350 °C, nitrogen as auxiliary and sheath gas (a pressure of 35 psi).

The data were collected using the Xcalibur 2.2.0 software (Thermo Scientific, USA). A control method to compare the trend was used to evaluate the obtained chromatograms in the SIEVE 2.1 software (Thermo Scientific, USA) according to the following parameter settings: a framing of 0–30 min, an *m/z* of 80–1000 Da, a frame time width of 0.5–1.5 min, an *m/z* width of 10 ppm, a threshold of 100 k counts, and a frame maximum of 5–50 k counts. To identify molecules (metabolites) in the selected frames, Human Metabolome Database [39] was used.

2.7. Statistical evaluation

The obtained spectral data were evaluated by linear discriminant analysis (LDA) in the XLSTAT software (Addinsoft, France) to distinguish between the AD patients and non-demented elderly controls. Statistical models were created for selected spectral regions that comprise significant information about the structure of proteins and other biomolecules in blood plasma. The performance of the models was expressed as sensitivity and specificity. Leave-one-out cross-validation [40,41] was carried out and receiver operator characteristics (ROC) [42] was analysed to verify the reliability of the results.

3. Results and discussion

3.1. Electronic circular dichroism

In the average ECD spectra (Fig. 1), three distinct bands were observed. The positive band at 192 nm as well as the negative band at 209 nm arise from the π-π*, whereas the negative 222-nm band reflects the n-π* electronic transitions of the peptide bond in peptides and proteins [43]. The band intensity and shape depend on peptide backbone geometry, in this case indicating a predominating α-helical conformation [27,44]. Although the highest contribution thereto may be ascribed to human serum albumin, the most abundant plasmatic protein adopting the α-helix, other plasmatic peptides/proteins are also partly responsible [45]. The lower intensity of the patient spectrum may; therefore, correlate with the decrease of albumin and other α-helical peptides/proteins or their partial misfolding during AD-related pathological states.

3.2. Raman optical activity

The mainly α-helical protein/peptide structure was also reflected in the ROA spectra (Fig. 2), specifically at 1630–1680 cm^{-1} (amide I; C=O stretch of the peptide bond) and 1230–1350 cm^{-1} (extended amide III; a combination of N—H and C_α—H bending with C_α—N stretching of the peptide bond) [27,46,47]. With AD progression, we observed not only an intensity increase of the negative band at 1645 cm^{-1}, but also a slight decrease at 1674 cm^{-1}. In addition, the presence of a broad band at 1309 cm^{-1} in comparison with its structured appearance in the case of EC, and a slight intensity increase within the negative band at 1247 cm^{-1} suggest a raising contribution of β-components [48] during AD pathogenesis.

The prominent positive bands at 1157 and 1516 cm^{-1} are associated with carotenoids overlapping with the bands of aromatic amino acid residues [27]. The depletion of carotenoids (demonstrated by a significant intensity decrease in the carotenoid-related spectral regions) is regarded a clear sign of oxidative stress highly contributing to the development and progression of AD. Furthermore, we identified variations within bands at 897 and 943 cm^{-1} confirming the prevailing α-helical conformation of plasmatic proteins/peptides [47,49], or a negative band at 1445 cm^{-1} related to CH_2 bending of aliphatic side-chain moieties (typically of peptides/proteins) or lipids/phospholipids.

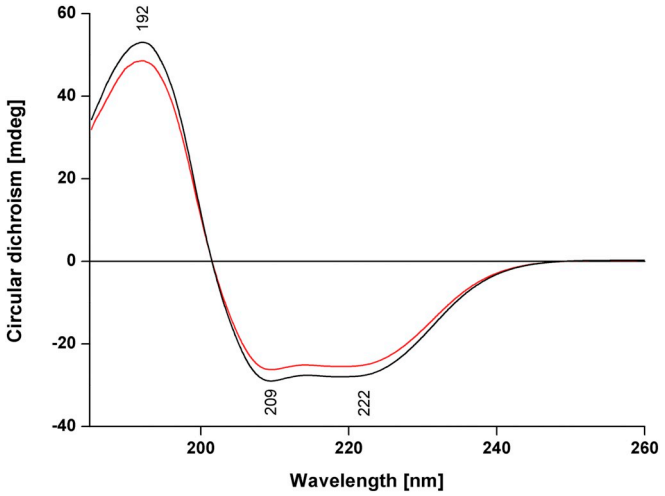

Fig. 1. Average ECD spectra of the blood plasma of patients with Alzheimer's disease (red; n = 35) and non-demented elderly controls (black; n = 29). (For interpretation of the references to colour in this figure legend, the reader is referred to the web version of this article.)

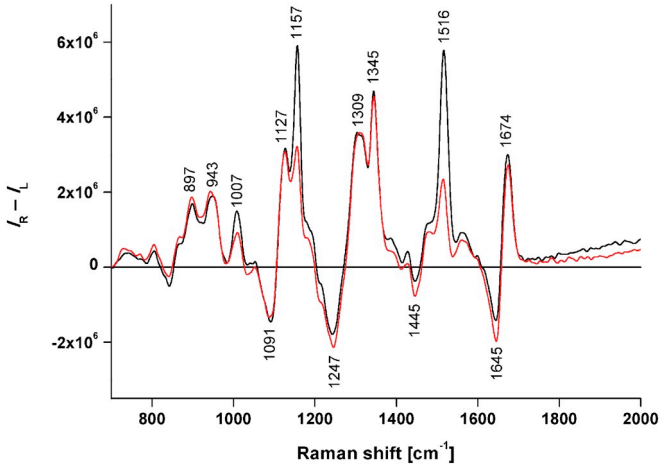

Fig. 2. Average ROA spectra of the blood plasma of patients with Alzheimer's disease (red; n = 35) and non-demented elderly controls (black; n = 29). (For interpretation of the references to colour in this figure legend, the reader is referred to the web version of this article.)

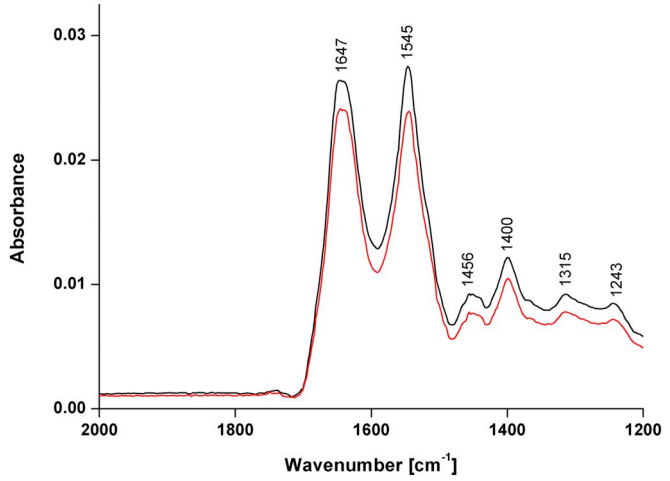

Fig. 3. Average IR spectra of the blood plasma of patients with Alzheimer's disease (red; $n = 35$) and non-demented elderly controls (black; $n = 29$). (For interpretation of the references to colour in this figure legend, the reader is referred to the web version of this article.)

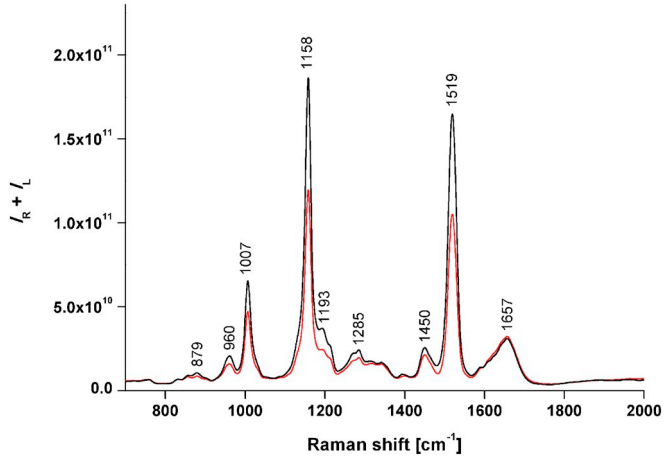

Fig. 4. Average Raman spectra of the blood plasma of patients with Alzheimer's disease (red; $n = 35$) and non-demented elderly controls (black; $n = 29$). (For interpretation of the references to colour in this figure legend, the reader is referred to the web version of this article.)

Table 1
Assignment of spectral bands selected for LDA [26,27,33].

Method	Band position	Assignment
ECD	192 nm	π-π* transition of the peptide bond in proteins
	209 nm	π-π* transition of the peptide bond in proteins
	222 nm	n-π* transition of the peptide bond in proteins
ROA	897 cm^{-1}	ν(CC), ν(CN); peptide backbone in proteins
	1247 cm^{-1}	δ(N−H), δ(C−H); amide III in proteins
	1345 cm^{-1}	δ(N−H), δ(C−H); amide III in proteins
	1445 cm^{-1}	δ(CH_3), δ(CH_2); lipids, aliphatic protein side chains
	1645 cm^{-1}	ν(C=O); amide I in proteins
	1675 cm^{-1}	ν(C=O); amide I in proteins
IR	1243 cm^{-1}	$\nu_{as}(PO^{2-})$; phospholipids
	1400 cm^{-1}	ν(COO^-); proteins, cholesterol
	1545 cm^{-1}	ν(CN), δ(N−H); amide II in proteins
	1647 cm^{-1}	ν(C=O); amide I in proteins
Raman	879 cm^{-1}	skeletal C−C, C−N vibrations of the peptide backbone
	1193 cm^{-1}	δ(C−H); Trp, Phe
	1285 cm^{-1}	δ(N−H), δ(C−H); amide III in proteins
	1450 cm^{-1}	δ(C−H); lipids, aliphatic side chains
	1588 cm^{-1}	ν(C−C); Tyr, Trp, Phe

Table 2
Confusion matrix of LDA cross-validation for patients with Alzheimer's disease and non-demented elderly controls.

From\to	AD	EC	Total	Correct
Alzheimer's disease	34	2	36	94%
Non-demented elderly controls	5	24	29	83%
Total	39	26	65	89%

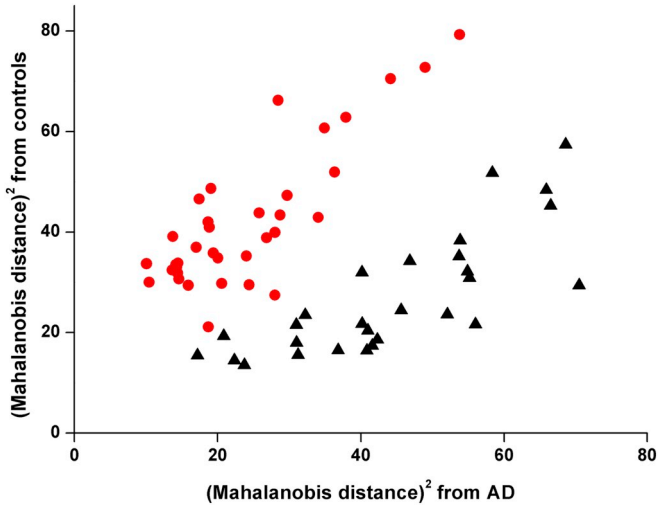

Fig. 5. Graphical representation of LDA for the combination of ECD, ROA, IR and Raman spectral data of patients with AD (●; $n = 35$) and non-demented elderly controls (▲; $n = 29$). The results are plotted in squared Mahalanobis distances to emphasize the within- and between-group differences. (For interpretation of the references to color in this figure legend, the reader is referred to the web version of this article.)

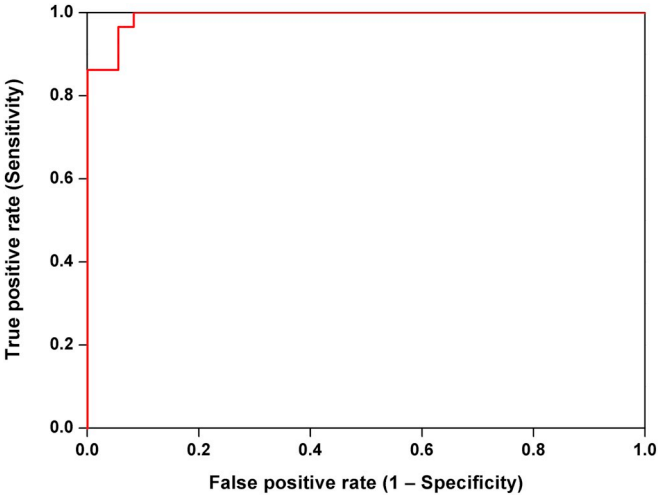

Fig. 6. ROC curve of the LDA model distinguishing between AD patients and non-demented elderly controls; AUC = 0.991.

3.3. Infrared spectroscopy

The IR spectra (Fig. 3) showed two pronounced bands at 1647 and 1545 cm^{-1} arising from the C=O stretching in the amide I, and from a combination of N−H bending and C_α−N stretching within the amide II regions, respectively. The type and content of protein secondary structure significantly influence the intensity and shape of these two bands [50,51]. Regarding this fact, it may be stated that lower absolute intensity as well as a difference in the relative intensity of these two spectral bands between the AD patients and EC may point out to

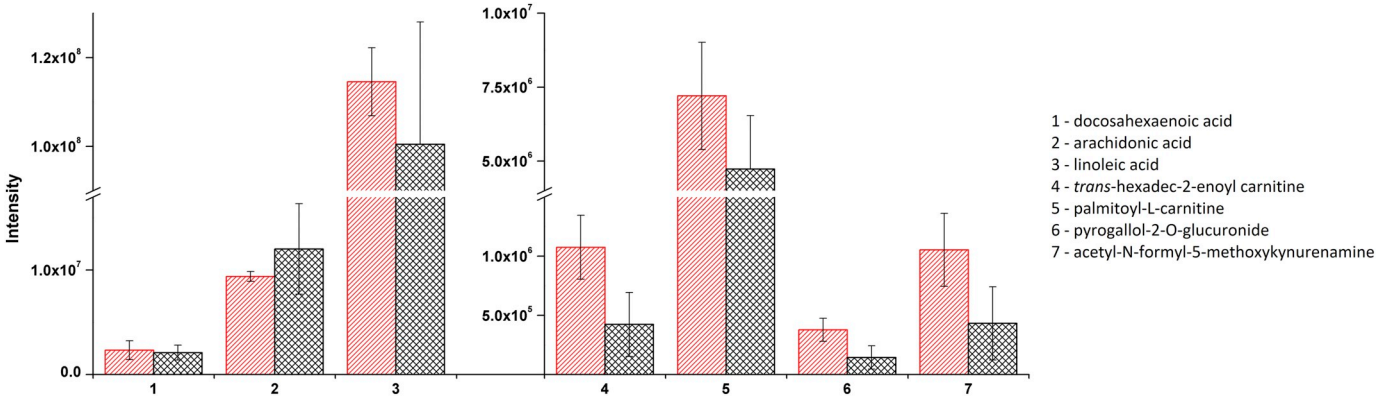

Fig. 7. Average intensities of the *m/z* signal of metabolites identified in the blood plasma of patients with Alzheimer's disease (hatched, red) and non-demented elderly controls (cross-hatched, black). (For interpretation of the references to colour in this figure legend, the reader is referred to the web version of this article.)

variations in the content and secondary structure of plasmatic proteins/peptides. The trend of intensity decrease was also observed for other studied regions, e.g. 1456 cm^{-1} (CH_2 and CH_3 bending of phospholipids and protein side-chain moieties) and 1240–1400 cm^{-1} (phospholipids overlapping with COO^- stretching of proteins and with cholesterol) [52].

3.4. Raman spectroscopy

In the average Raman spectra (Fig. 4), the most prominent bands (1007, 1158 and 1519 cm^{-1} represent the C—C and C═C vibrations of carotenoids [27,53]. Their intensity is enhanced due to the use of a visible excitation (532 nm) [53,54]. Although plasma carotenoid levels slightly decrease during aging, the notably lower intensities of the carotenoid spectral bands in the group of AD patients may also suggest their utilization for protection against oxidative stress. Furthermore, the decreased carotenoid levels in AD may be caused by disruptions in lipid metabolism, which lead to lower carotenoid release from the adipose tissue, their natural storage.

No differences were observed for the amide I band at 1657 cm^{-1}, but intensity decrease was detected within the more conformation-sensitive amide III region, specifically at 1270 and 1285 cm^{-1}. This may again indicate an AD-induced structural change in proteins/peptides (partial misfolding) leading to the loss of biological function. Further intensity variations were noticed in the bands of side-chain CH_2 and CH_3 groups (1450 cm^{-1}; overlap with phospholipids), alanine and tryptophan residues (1007 cm^{-1} overlapping with carotenoids, and 1193 cm^{-1}) [27].

3.5. Linear discriminant analysis

To assess the performance characteristics (sensitivity, specificity) of our approach, the obtained data sets were subjected to a statistical evaluation. A combination of selected spectral bands (Table 1) from all utilized techniques allowed for a discrimination of patients and controls with an overall accuracy of 89% (after cross-validation; Table 2). Although two AD patients and five EC were misclassified in cross-validation, the studied groups did not significantly overlap (Fig. 5). Moreover, sensitivity and specificity remained high even after the cross-validation, *i.e.* 94% and 83%, respectively, implying that the observed spectral features may be considered potential AD markers. The reliability of the applied approach was illustrated by a high area under the ROC curve, reaching 0.991 (Fig. 6).

3.6. Metabolomics

By metabolomics, we monitored disease-induced changes in plasmatic molecules smaller than proteins, typically with a mass lower than 2000 Da. Apart from traditional markers of inflammation (docosahexaenoic, arachidonic, linoleic acid) or the disruption of fatty acid/lipid metabolism (*trans*-hexadec-2-enoyl carnitine, palmitoyl-L-carnitine) [39], we also identified metabolites, whose connection with AD was not yet studied (pyrogallol-2-O-glucuronide, acetyl-N-formyl-5-methoxykynurenamine). The comparison of the *m/z* intensities of the aforementioned metabolites between the patient and control groups is plotted in Fig. 7.

Essential fatty acids, such as docosahexaenoic, arachidonic and linoleic acid, play an important role in membrane integrity and energy management of the cell [39]. Under physiological conditions, linoleic acid undergoes a metabolic transformation to arachidonic acid [39,55]. However according to our findings (increase in linoleic acid while arachidonic acid decreased), this does not apparently happen during AD, meaning that the metabolism of fatty acids may be disturbed. In addition, the reduced level of arachidonic acid may point to insulin resistance strongly affecting glucose management, which is also believed to have a connection with AD [56,57].

Similarly, the higher *m/z* intensity of *trans*-hexadec-2-enoyl carnitine and palmitoyl-L-carnitine also suggests a disruption of fatty acid metabolism during AD development, as both of these substances take part primarily in lipid and fatty acid management [39]. Excessive amounts of palmitoyl-L-carnitine itself may strongly influence cell membrane fluidity, thereby changing the activity of membrane enzymes and transporters [58]. Moreover, palmitoyl-L-carnitine is assumed to alter the activity of proteins [39], leading to disturbances in their correct biological function and possibly to the development of protein-misfolding diseases, such as AD.

Pyrogallol is considered highly toxic and; thus, it is bound by glucuronic acid to form a water-soluble waste product (pyrogallol-2-O-glucuronide), which is then easily excreted in urine. Despite its toxicity, pyrogallol is also able to bind oxygen [39]. Therefore, the increased level of pyrogallol-2-O-glucuronide found in the AD patients may reflect the attempt of the body to fight reactive oxygen species, which cause oxidative stress inevitably leading to neuronal damage.

Acetyl-N-formyl-5-methoxykynurenamine (AFMK) is a by-product of melatonin metabolism and exhibits strong immunomodulatory properties [39]. Enormously elevated levels thereof were found in the CSF and blood of patients suffering from meningitis [59], which suggests a certain role of AFMK in the process of brain inflammation. Here, we observed a significantly higher intensity of AFMK in the patient plasma than in controls, which indicates the presence of brain inflammation, one of the basic neuropathological features of AD.

4. Conclusions

We successfully identified the spectral signature of Alzheimer's disease using an uncommon combination of highly-sensitive polarized

and non-polarized techniques of molecular spectroscopy. The observations indicated that not only protein concentration, but also structure varies with the disease development. Furthermore, the decrease of Raman/ROA carotenoid bands within the patient group suggested their role in the elimination of excessive oxidative stress occurring in AD, and confirmed disturbances of lipid metabolism. The statistical analysis of the acquired spectral data allowed for a highly accurate discrimination between the studied groups, with sensitivity and specificity (94% and 83%, respectively) exceeding the clinical requirements for an ideal biomarker. Additional metabolomic profiling confirmed disturbances of fatty acid/lipid metabolism (linoleic acid, palmitoyl-L-carnitine), the evidence of which was also observed *via* spectroscopy. Moreover, we identified a metabolite (acetyl-N-formyl-5-methoxykynurenamine) involved in inflammatory processes within the brain, which has not been linked to AD. Thus, the achieved results showed strong potential of the unique combination of spectroscopy and metabolomics to become reliable tools in AD diagnosis while being minimally invasive.

Conflicts of interest

The authors have no conflicts of interest to declare.

Acknowledgements

This study was financially supported by the Czech Science Foundation (17-05292S).

References

[1] M. Prince, A. Wimo, M. Guerchet, G.-C. Ali, Y.T. Wu, M. Prina, World Alzheimer Report 2015. The Global Impact of Dementia. An Analysis of Prevalence, Incidence, Cost and Trends, Alzheimer's Disease Iternational, London, 2015.
[2] A. Wimo, M. Guerchet, G.-C. Ali, Y.-T. Wu, M. Prina, B. Winblad, L. Jönsson, Z.M. liu, M. Prince, Alzheimers Dement. 13 (1) (2017).
[3] C.G. Liu, T. Kanekiyo, H. Xu, G. Bu, Nat. Rev. Neurol. (9) (2013) 106.
[4] Alzheimer's Association, Alzheimer's Dement. vol. 12, (2016), p. 459.
[5] P.T. Francis, A.M. Palmer, M. Snape, G.K. Wilcock, J. Neurol. Neurosurg. Psychiatry 66 (1999) 137.
[6] S.H. Barage, K.D. Sonawane, Neuropeptides 52 (2015) 1.
[7] R.A. Stelzmann, H.N. Schnitzlein, F.R. Murtagh, Clin. Anat. 8 (1995) 429.
[8] G. Verdile, S. Fuller, C.S. Atwood, S.M. Laws, S.E. Gandy, R.N. Martins, Pharmacol. Res. 50 (2004) 347.
[9] Z. Nagy, M.M. Esiri, K.A. Jobst, J.H. Morris, E.M. King, B. McDonald, S. Litchfield, A. Smith, L. Barnetson, A.D. Smith, Dementia 6 (1995) 21.
[10] R.B. Maccioni, G. Farias, I. Morales, L. Navarette, Arch. Med. Res. 41 (2010) 226.
[11] R.H. Swerdlow, S.M. Khan, Med. Hypotheses 63 (2004) 8.
[12] D. Praticó, Trends Pharmacol. Sci. 29 (2008) 609.
[13] C.R. Jack, M.S. Albert, D.S. Knopman, G.M. McKhann, R.A. Sperling, M.C. Carrillo, B. Thies, C.H. Phelps, Alzheimers Dement. 7 (2011) 257.
[14] C.R. Jack, D.S. Knopman, W.J. Jagust, L.M. Shaw, P.S. Aisen, M.W. Weiner, R.C. Petersen, J.Q. Trojanowski, Lancet Neurol. 9 (2010) 119.
[15] K.A. Johnson, N.C. Fox, R.A. Sperling, W.E. Klunk, Cold Spring Harb. Perspect. Med. 2 (2012) a006213.
[16] E.C. van Straaten, P. Scheltens, F. Barkhof, J. Neurol. Sci. 226 (2004) 9.
[17] D.M. Walsh, D.J. Selkoe, J. Neurochem. 101 (2007) 1172.
[18] M. Griebe, M. Daffertshofer, M. Stroick, M. Syren, P. Ahmad-Nejad, M. Neumaier, J. Backhaus, M.G. Hennerici, M. Fatar, Neurosci. Lett. 420 (2007) 29.
[19] G. Zuliani, M. Cavalieri, M. Galvani, A. Passaro, M.R. Miunari, C. Bosi, A. Zurlo, R. Fellin, J. Neurol. Sci. 272 (2008) 164.
[20] T. Tukiainen, T. Tynkkynen, V.P. Makinen, P. Jylanki, A. Kangas, J. Hokkanen, A. Vehtari, O. Grohn, M. Hallikainen, H. Soininen, M. Kivipelto, P.H. Groop, K. Kaski, R. Laatikainen, P. Soininen, T. Pirttila, M. Ala-Korpela, Biochem. Biophys. Res. Commun. 375 (2008) 356.
[21] M.J. Baker, S.R. Hussain, L. Lovergne, V. Untereiner, C. Hughes, R.A. Lukaszewski, G. Thiéfin, G.D. Sockalingum, Chem. Soc. Rev. 45 (2016) 1803.
[22] P. Lasch, J. Kneipp (Eds.), Biomedical Vibrational Spectroscopy, John Wiley & Sons, Inc., New York, 2008.
[23] J. Lopes, M. Correia, I. Martins, A.G. Henriques, I. Delgadillo, O. da Cruz e Silva, A. Nunes, J. Alzheimers Dis. 52 (2016) 801.
[24] A. Nabers, J. Ollesch, J. Schartner, C. Kötting, J. Genius, U. Haußmann, H. Klafki, J. Wiltfang, K. Gerwert, J. Biophotonics 9 (2016) 224.
[25] E. Peuchant, S. Richard-Harston, I. Bourdel-Marchasson, J.F. Dartigues, L. Letenneur, P. Barberger-Gateau, S. Arnaud-Dabernat, J.Y. Daniel, Transl. Res. 152 (2008) 103.
[26] M. Tatarkovič, Z. Fišar, J. Raboch, R. Jirák, V. Setnička, Chirality 24 (2012) 951.
[27] A. Synytsya, M. Judexová, T. Hrubý, M. Tatarkovič, M. Miškovičová, L. Petruželka, V. Setnička, Anal. Bioanal. Chem. 405 (2013) 5441.
[28] M. Tatarkovič, A. Synytsya, L. Šťovíčková, B. Bunganič, M. Miškovičová, L. Petruželka, V. Setnička, Anal. Bioanal. Chem. 407 (2015) 1335.
[29] V. Setnička, L. Habartová, P.L. Polavarapu (Ed.), Chiral Analysis. Advances in Spectroscopy, Chromatography and Emerging Methods, 2nd edn, Elsevier, Cambridge, USA, 2018, , https://doi.org/10.1016/B978-0-444-64027-7.00010-2 ch. 10, pp. 429.
[30] N. Berova, K. Nakanishi, P.L. Polavarapu, R.W. Woody (Eds.), Comprehensive Chiroptical Spectroscopy: Applications in Stereochemical Analysis of Synthetic Compounds, Natural Products, and Biomolecules, John Wiley & Sons Inc., Hoboken, New Jersey, 2012.
[31] L.A. Nafie, Vibrational Optical Activity, John Wiley & Sons, Inc, Chichester, 2011.
[32] P.L. Polavarapu, Chiroptical Spectroscopy: Fundamentals and Applications, CRC Press, Boca Raton, 2016.
[33] L.D. Barron, Biomed. Spectrosc. Imaging 4 (2015) 223.
[34] L. Šťovíčková, M. Tatarkovič, H. Logerová, J. Vavřinec, V. Setnička, Analyst 140 (2015) 2266.
[35] M. Tatarkovič, M. Miškovičová, L. Šťovíčková, A. Synytsya, L. Petruželka, V. Setnička, Analyst 140 (2015) 2287.
[36] L. Habartová, B. Bunganič, M. Tatarkovič, M. Zavoral, J. Vondroušová, K. Syslová, V. Setnička, Chirality 30 (2018) 581.
[37] M.F. Folstein, S.E. Folstein, P.R. McHugh, J. Psychiatr. Res. 12 (1975) 189.
[38] M. Člupek, P. Matějka, K. Volka, J. Raman Spectrosc. 38 (2007) 1174.
[39] D.S. Wishart, T. Jewison, A.C. Guo, M. Wilson, C. Knox, Y. Liu, Y. Djoumbou, R. Mandal, F. Aziat, E. Dong, S. Bouatra, I. Sinelnikov, D. Arndt, J. Xia, P. Liu, F. Yallou, T. Bjorndahl, R. Perez-Pineiro, R. Eisner, F. Allen, V. Neveu, R. Greiner, A. Scalbert, Nucleic Acids Res. 41 (2013) D801.
[40] C. Sammut, G.I. Webb (Eds.), Encyclopedia of Machine Learning, Springer, New York, 2010.
[41] R.A. Dunne, R.A. Dunne (Ed.), A Statistical Approach to Neural Networks for Pattern Recognition, John Wiley & Sons, Inc., New Jersey, 2006, p. 19, , https://doi.org/10.1002/9780470148150.ch3.
[42] T. Fawcett, Pattern Recogn. Lett. 27 (2006) 861.
[43] R.W. Woody, N. Berova, K. Nakanishi, P.L. Polavarapu, R.W. Woody (Eds.), Comprehensive Chiroptical Spectroscopy: Applications in Stereochemical Analysis of Synthetic Compounds, Natural Products, and Biomolecules, vol. 2, John Wiley & Sons, New Jersey, 2012, p. 475.
[44] L. Whitmore, B.A. Wallace, Biopolymers 89 (2008) 392.
[45] R.K. Murray, D.A. Bender, K.M. Botham, P.J. Kennelly, V.W. Rodwell, P.A. Weil, Harper's Illustarted Biochemistry, McGraw-Hill, New York, 2003.
[46] F. Zhu, N.W. Isaacs, L. Hecht, L.D. Barron, Structure 13 (2005) 1409.
[47] L.D. Barron, F. Zhu, L. Hecht, G.E. Tranter, N.W. Isaacs, J. Mol. Struct. 7 (2007) 834–836.
[48] M.N. Kinalwa, E.W. Blanch, A.J. Doig, Anal. Chem. 82 (2010) 6347.
[49] F. Zhu, N.W. Isaacs, L. Hecht, G.E. Tranter, L.D. Barron, Chirality 18 (2006) 103.
[50] I. Daidone, M. Aschi, L. Zanetti-Polzi, A. Di Nola, A. Amadei, Chem. Phys. Lett. 488 (2010) 213.
[51] P. Carmona, M. Molina, M. Calero, F. Bermejo-Pareja, P. Martinez-Martin, I. Alvarez, A. Toledano, Anal. Bioanal. Chem. 402 (2012) 2015.
[52] J.A.A.C. Piva, J.L.R. Silva, L. Raniero, A.A. Martin, H.G. Bohr, K.J. Jalkanen, Theor. Chem. Accounts 130 (2011) 1261.
[53] R. Withnall, B.Z. Chowdhry, J. Silver, H.G.M. Edwards, L.F.C. de Oliveira, Spectrochim. Acta A 59 (2003) 2207.
[54] S.F. Parker, S.M. Tavender, N.M. Dixon, H.K. Herman, K.P.J. Williams, W.F. Maddams, Appl. Spectrosc. 53 (1999) 86.
[55] G.F. Hoffmann, W. Meier-Augenstein, S. Stockler, R. Surtees, D. Rating, W.L. Nyhan, J. Inherit. Metab. Dis. 16 (1993) 648.
[56] W.Q. Zhao, M. Townsend, Biochim. Biophys. Acta 1792 (2009) 482.
[57] Y. Yang, W. Song, Neuroscience 250 (2013) 140.
[58] H. Watanabe, A. Kobayashi, H. Hayashi, N. Yamazako, Biochim. Biophys. Acta 980 (1989) 315.
[59] S.O. Silva, V.F. Ximenes, J.A. Livramento, L.H. Catalani, J. Pineal Res. 39 (2005) 302.